PLOS COMPUTATIONAL BIOLOGY

RESEARCH ARTICLE

Computational simulation of the reactive oxygen species and redox network in the regulation of chloroplast metabolism

Melanie Gerken[1], **Sergej Kakorin**[2], **Kamel Chibani**[1], **Karl-Josef Dietz**[1]*

1 Department of Biochemistry and Physiology of Plants, Faculty of Biology, Bielefeld University, Bielefeld, Germany, **2** Physikalische Chemie III, Faculty of Chemistry, Bielefeld University, Bielefeld, Germany

* karl-josef.dietz@uni-bielefeld.de

Citation: Gerken M, Kakorin S, Chibani K, Dietz K-J (2020) Computational simulation of the reactive oxygen species and redox network in the regulation of chloroplast metabolism. PLoS Comput Biol 16 (1): e1007102. https://doi.org/10.1371/journal.pcbi.1007102

Editor: Pedro Mendes, University of Connecticut School of Medicine, UNITED STATES

Received: May 10, 2019

Accepted: August 15, 2019

Published: January 17, 2020

Data Availability Statement: All relevant data are within the manuscript and its Supporting Information files.

Funding: This work was supported by the Deutsche Forschungsgemeinschaft (DI346/17). The funders had no role in study design, data collection and analysis, decision to publish, or preparation of the manuscript.

Competing interests: The authors have no competing interest.

Abstract

Cells contain a thiol redox regulatory network to coordinate metabolic and developmental activities with exogenous and endogenous cues. This network controls the redox state and activity of many target proteins. Electrons are fed into the network from metabolism and reach the target proteins via redox transmitters such as thioredoxin (TRX) and NADPH-dependent thioredoxin reductases (NTR). Electrons are drained from the network by reactive oxygen species (ROS) through thiol peroxidases, e.g., peroxiredoxins (PRX). Mathematical modeling promises access to quantitative understanding of the network function and was implemented by using published kinetic parameters combined with fitting to known biochemical data. Two networks were assembled, namely the ferredoxin (FDX), FDX-dependent TRX reductase (FTR), TRX, fructose-1,6-bisphosphatase (FBPase) pathway with 2-cysteine PRX/ROS as oxidant, and separately the FDX, FDX-dependent NADP reductase (FNR), NADPH, NTRC-pathway for 2-CysPRX reduction. Combining both modules allowed drawing several important conclusions of network performance. The resting H_2O_2 concentration was estimated to be about 30 nM in the chloroplast stroma. The electron flow to metabolism exceeds that into thiol regulation of FBPase more than 7000-fold under physiological conditions. The electron flow from NTRC to 2-CysPRX is about 5.32-times more efficient than that from TRX-f1 to 2-CysPRX. Under severe stress (30 μM H_2O_2) the ratio of electron flow to the thiol network relative to metabolism sinks to 1:251 whereas the ratio of e^- flow from NTRC to 2-CysPRX and TRX-f1 to 2-CysPRX rises up to 1:67. Thus, the simulation provides clues on experimentally inaccessible parameters and describes the functional state of the chloroplast thiol regulatory network.

Author summary

The state of the thiol redox regulatory network is a fundamental feature of all cells and determines metabolic and developmental processes. However, only some parameters are quantifiable in experiments. This paper establishes simplified mathematical models which enable simulation of electron flows through the regulatory system. This in turn allows for

estimating rates and states of components of the network and to tentatively address previously unknown parameters such as the resting hydrogen peroxide levels or the expenditure of reductive power for regulation relative to metabolism. The establishment of such models for simulating the performance and dynamics of the redox regulatory network is of significance not only for photosynthesis but also, e.g., in bacterial and animal cells exposed to environmental stress or pathological disorders.

Introduction

Reduction-oxidation reactions drive life. In aerobic metabolism, electrons from reduced compounds pass on to oxygen to produce water and ATP. Photosynthesis exploits light energy and reverses this oxidation process by water splitting, liberation of O_2 and reduction of CO_2, NO_3^- and SO_4^{2-} to carbohydrates, amines and sulfhydryl compounds. A decisive role is played by ferredoxin (FDX) which functions as hub of electron distribution accepting electrons from photosystem I and donating them in particular to FDX-dependent NADP reductase (FNR), FDX-dependent nitrite reductase (NIR), FDX-dependent sulfite reductase (SIR), FDX-dependent glutamate oxoglutarate aminotransferase (GOGAT), FDX-dependent thioredoxin reductase (FTR) and to O_2 in the Mehler reaction [1]. Considering the elemental composition of a typical plant body, C:N:S need to reduced and incorporated at a ratio of roughly 40:8:1. Fine-tuned regulation of electron flows and metabolism is needed to realize the proper ratio and to avoid futile cycles.

The adjustment of metabolic fluxes in the chloroplast to a major extent is controlled by electron flow into the thiol redox regulatory network. Polypeptides switch from an oxidized form with intra- or intermolecular disulfide bridges to a reduced thiol state. TRX and the chloroplast NADPH-dependent TRX reductase C (NTRC) act as electron transmitters in the reduction process. NTRC combines a NADPH-dependent TRX reductase domain with a TRX domain [2]. The TRX complement of Arabidopsis plastids comprises 20 TRX and TRX-like proteins with representatives of the f-, m-, x-, y-, z-group of TRX, TRX-like proteins which include chloroplast drought-induced stress protein of 32 kDa (CDSP32), Lilium1-4 (ACHT1-4) and TRX-like [3].

TRX-f1 and TRX-f2 function in activation of Calvin-Benson-Bassham cycle (CBB) enzymes and γ-subunit of F-ATP synthase [4]. TRX-m1, -m2, -m3 and–m4 are suggested to regulate targets which control the NADPH/NADP ratio [5] which is linked to their ability to efficiently activate the NADPH-dependent malate dehydrogenase [6]. TRX-x, NTRC and TRX-lilium1 (ACHT4a) were identified as reductants of the 2-cysteine peroxiredoxin (2CysPRX) [7–9], and TRX-y1 and–y2 as reductant of PRX-Q [10]. These exemplary studies describe specificity and redundancy for the interaction between TRX-forms and target proteins, as, e.g., comparatively investigated by Collin et al. [7].

Upon transition from dark to light or upon an increase in photosynthetic active radiation (PAR) reductive activation of CBB enzymes via redox sensitive thiols stimulates consumption of NADPH and ATP and coordinates energy provision in the photosynthetic electron transport (PET) chain and energy consumption in metabolic pathways [3,4]. However it is less understood how once activated enzymes are down-regulated by oxidation. Oxygen and reactive oxygen species (ROS) function as final electron acceptors. ROS generated in the PET react with thiol peroxidases (TPX) with high affinity [11]. Redox transmitters regenerate oxidized TPX. In case of 2CysPRX, NTRC most efficiently reduces the oxidized form. Other redox

transmitters such as TRX-f1, Trx-m1 or Trx-like proteins like CDSP32 also reduce 2CysPRX at lower rates [7].

The main pathway of TRX reduction targets proteins via FDX and FTR and prevails in strong light. In addition NTRC provides electrons to 2CysPRX which compensates for the oxidation of 2CysPRX by PET-produced hydrogen peroxide (H_2O_2) [2]. The drainage of electrons from other TRXs to oxidized 2CysPRX may be insignificant under these conditions. This situation changes in darkness were the rate through the PET-driven FDX/TRX-pathway mostly ceases, or at lowered photosynthetic active radiation where intermediate flux conditions are established. This balance between oxidation and reduction is suggested to determine the rate of, e.g., the CBB [12].

Thiol-redox regulation in the chloroplast addresses multiple metabolic processes and pathways and there exist examples of oxidative activation of protein functions. Thus TRXs reductively inhibit the oxidative pentose phosphate cycle by inactivating the committed enzyme glucose-6-phosphate dehydrogenase [13].

While the experimental evidence supports the functionality of this regulatory model, quantitative understanding of the interacting electron fluxes within the network cannot be obtained exclusively from experiments but requires mathematical simulation of the involved major pathways. For this reason this study aimed to first simulate individual electron pathways and then to combine them for predicting crucial parameters of the network inaccessible to experimental determination. Using this approach, it was possible to estimate relative electron fluxes directed into carbon reduction and thiol dependent regulation, and to estimate the rate of H_2O_2 production in the chloroplast.

Results

FDX functions as hub for electron distribution at the donor site of photosystem I. The first mathematical model aimed to simulate electron distribution from TRX-f1 to FBPase and 2CysPRX in dependence on the H_2O_2 concentration (Fig 1A) and was built on the model presented by Vaseghi et al. [12] which was expanded by including H_2O_2 and reversibility of the reactions in Eqs 1 and 2. The question asked concerned the efficiency of oxidized 2CysPRX to compete with reduction of TRX-f1 by FDX-dependent TRX reductase (FTR). The H_2O_2

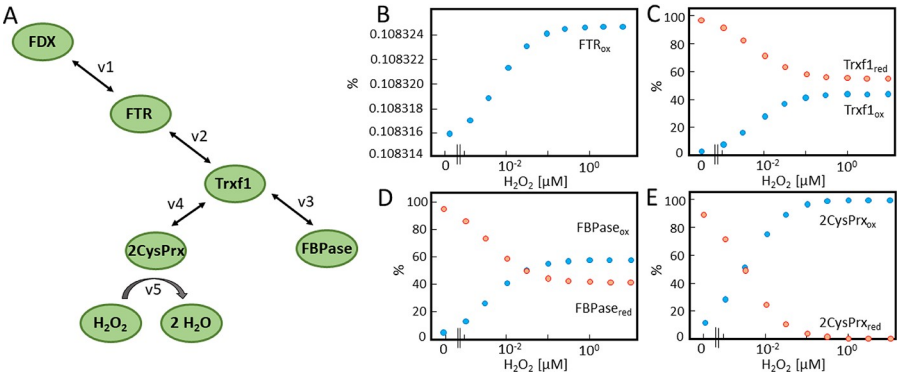

Fig 1. Simulated redox state of FTR-network components in dependence on H_2O_2 concentration. (A) Schematic representation of the FTR-network. Electrons are drained from FD through FTR and TRX-f1 to either FBPase or 2CysPRX which in turn is oxidized by H_2O_2. Each component switches between the reduced and oxidized state. The concentrations were calculated for 1 mg Chl (S1 Table). FDX was clamped to 50% reduced state. Starting values of FTR and TRX-f1 were set to 80% reduced and 20% oxidized. 2CysPRX start values for reduced and oxidized form were 35% and 65% [12]. (B-E) Redox states of the network components FTR, TRX-f1, 2CysPRX and FBPase at varying H_2O_2 concentrations as obtained after 3h of simulation in the presence of H_2O_2 ranging between 0 and 10 μM.

https://doi.org/10.1371/journal.pcbi.1007102.g001

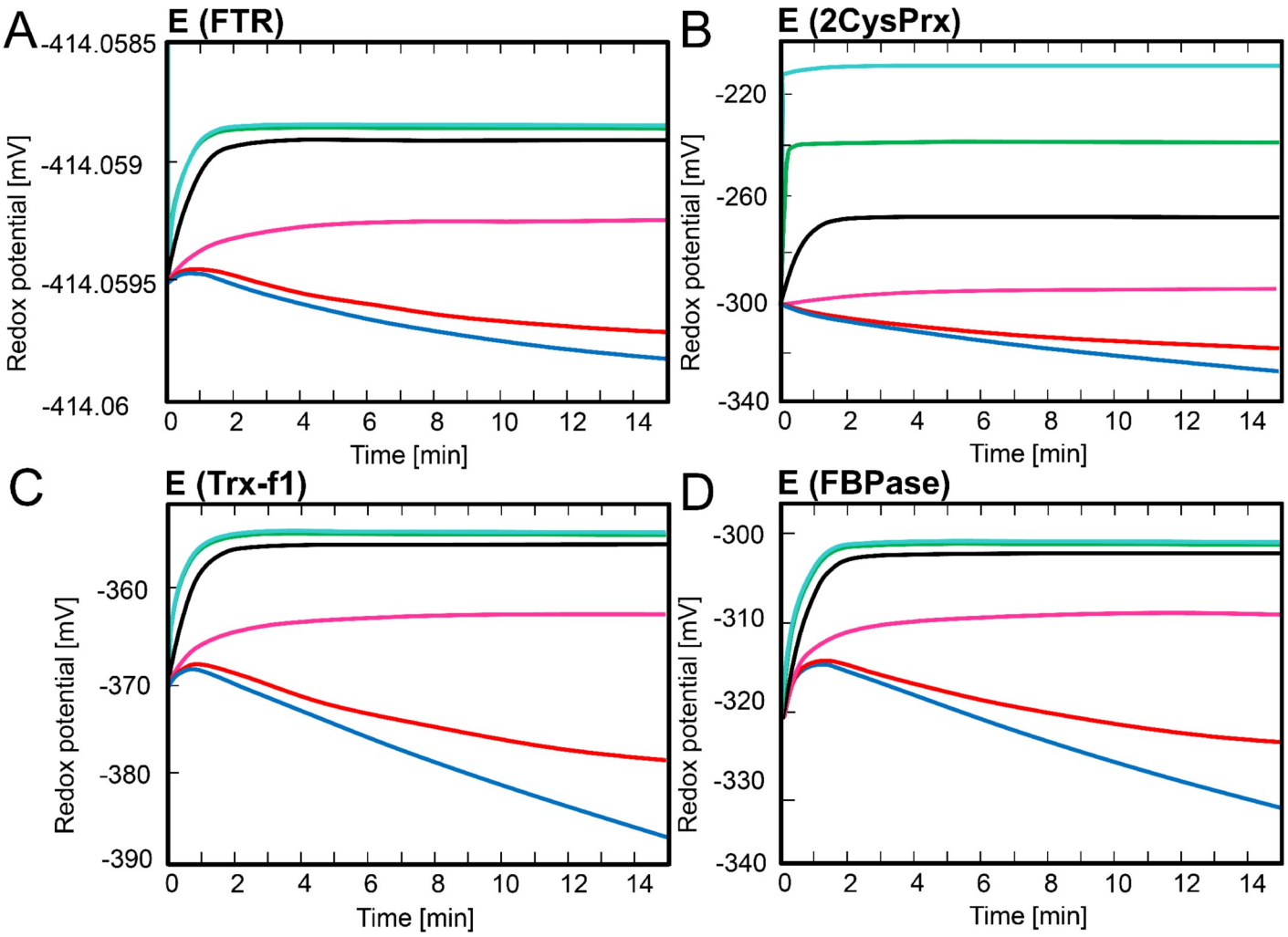

Fig 2. Time-dependent simulation of redox potential changes of FTR-network components. The redox potentials of FTR, TRX-f1, FBPase, 2CysPRX were simulated at varying H_2O_2 concentrations. Redox potentials were calculated at each time step using the Nernst equation for (A) FTR, (B) 2CysPRX, (C) TRX-f1 and (D) FBPase. The simulation was run for 15 min for each H_2O_2 concentration adjusted to 0 nM (blue), 1 nM (red), 10 nM (magenta), 100 nM (black), 1 μM (green) and 10 μM (cyan).

https://doi.org/10.1371/journal.pcbi.1007102.g002

concentration was adjusted to values between 0 and 10 μM and the steady state redox states of FTR, TRX-f1, FBPase and 2CysPRX were modelled by kinetic simulation (Fig 1B–1E). The FTR was highly reduced under all conditions and there was almost no increase in oxidation if the H_2O_2 rose from 1 nM to 100 nM. Further elevation of H_2O_2 had no further effect since the 2CysPRX turned maximally oxidized at 100 nM and higher H_2O_2 concentrations. In the same range, the oxidized form of TRX-f1 reached 44%, while the FBPase was oxidized by 58%.

Fig 2 depicts the time-dependent changes in redox potential of the sub-network components FTR, TRX-f1, FBPase and 2CysPRX. In the absence of H_2O_2 or at 1 nM, the starting condition shifted to a slightly more reduced state. On the contrary, the FBPase redox potential was poorly affected by increasing the H_2O_2 concentration from 1 to 10 μM and even 100 nM already strongly oxidized the TRX-f1 and FBPase proteins. Thus, this simple network simulation together with the reported ex vivo redox states of the components allowed us to predict that stromal H_2O_2 levels likely range somewhere between 1 and 100 nM.

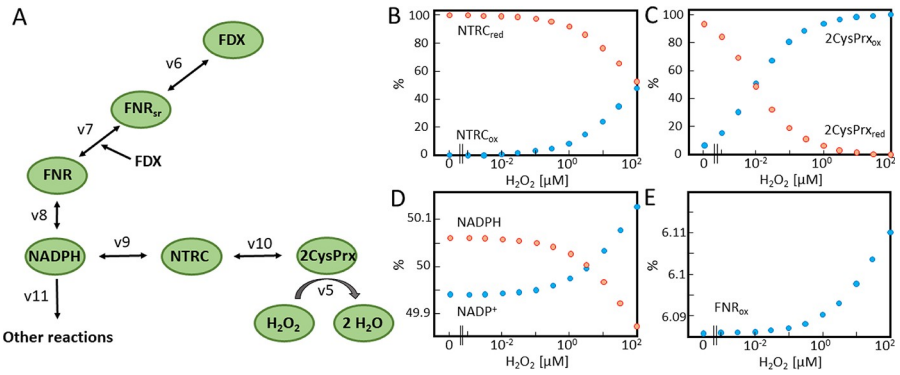

Fig 3. Simulated steady state concentration of FNR-network components at various H_2O_2 concentrations. (A) Schematic representation of FNR-network simulated in the second model. Here, electrons passed from FDX through FNR, $NADP^+$, NTRC to 2CysPRX and finally H_2O_2. Each component was able to adopt a reduced or oxidized state. FNR is represented in three states in the model; reduced (red), semi reduced (semired) and oxidized (ox). The physiological concentrations were calculated for 1 mg Chl (S2 Table). FDX was clamped to 50% reduction. Initial values of FNR_{red} and $FNR_{semired}$ were set to 40%. All other oxidized forms were initially set to 20% apart from 2CysPRX at the starting point with 65% in the oxidized form [12]. The NADPH/$NADP^+$ couple was full reduced at t = 0. To mimic metabolic NADPH oxidation an additional reaction constant (v7) was added. (B-E) The redox state of the network components (B) NTRC, (C) 2CysPRX, (D) NADPH, $NADP^+$ and (E) FNR_{ox}, was simulated for 3h at constant H_2O_2 concentrations varying from 0 µM to 100 µM.

https://doi.org/10.1371/journal.pcbi.1007102.g003

The second model was constructed to simulate the FNR branch of the network (Fig 3). Generated NADPH provided electrons to metabolism (v11) or to NTRC for reducing 2CysPRX. H_2O_2 was adjusted to concentrations between 0 and 100 µM. Fig 3B–3E depicts the relative redox forms computed for simulated time period of 3 h which essentially represents the final steady state. The most sensitive component of the network was 2CysPRX. At about 10 nM H_2O_2, the 2CysPRX was half reduced and half oxidized. NTRC and NADPH responded significantly, here considered as increase in oxidation by at least 10%, when H_2O_2 reached a concentration of 1 µM.

The simulation of the FNR-network presented in Fig 4 focused on the time-dependent changes in redox potentials. The increase of the clamped H_2O_2 concentration from 10 (magenta) to 100 nM (black) switched the trend from increased reduction, equivalent to more negative redox potentials, to more oxidation which is equivalent to less negative redox potentials.

In the next step, the FTR and FNR networks were combined (Fig 5A). The H_2O_2 concentration was clamped to values between 0 and 100 µM as before and the redox states of the components derived in the approximated steady state after 3h of simulation (Fig 5B–5I). The H_2O_2

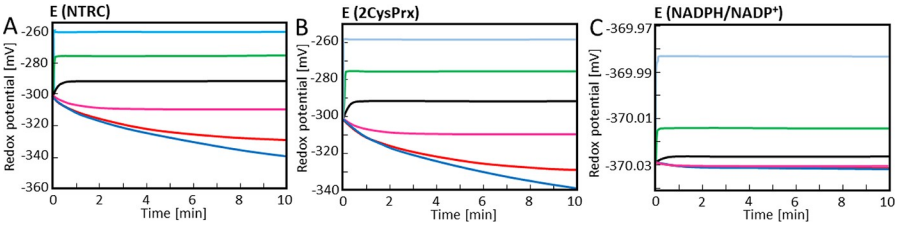

Fig 4. Time-dependent simulation of the redox potentials of the FNR-network components. The redox potentials were simulated for the FNR-network components FdX, FNR, NADPH, NTRC and 2CysPRX in dependence of the clamped H_2O_2 concentration. Redox potentials were calculated at each time step using Nernst equation for (A) NTRC, (B) 2CysPRX and (C) NADPH/$NADP^+$ couple. The simulation was run for 10 minutes at constant H_2O_2 concentration of 0 µM (blue), 1 nM (red), 10 nM (magenta), 100 nM (black), 1 µM (green) and 10 µM (cyan).

https://doi.org/10.1371/journal.pcbi.1007102.g004

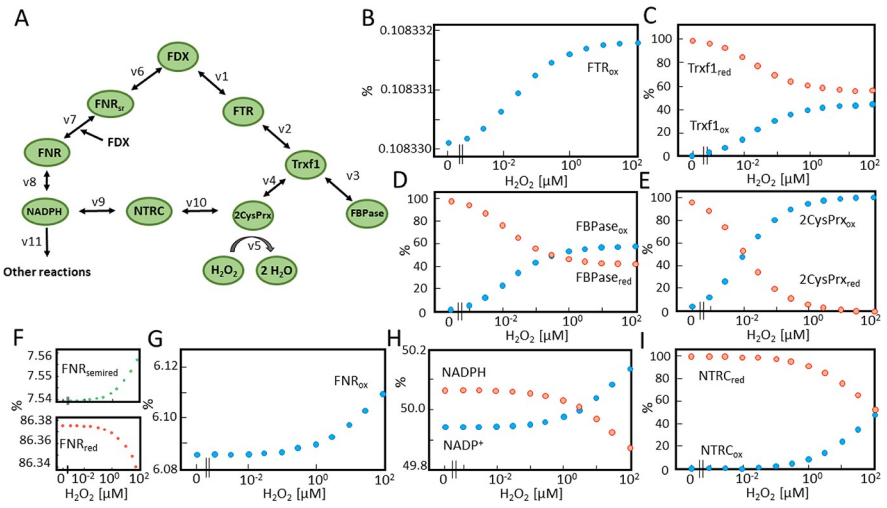

Fig 5. Simulation in the combined model of the redox states of the chloroplast FTR/FNR-network components in the presence of varying H_2O_2 concentrations. (A) Schematic representation of the combined FTR/FNR-network model. Electrons from FDX could flow either through the FNR branch to $NADP^+$ and NTRC or were transported through the FTR branch to TRX-f1 and FBPase. Thus electrons were transferred to 2CysPRX and H_2O_2 by NTRC and TRX-f1. Each component adopted either a reduced or oxidized state. FNR is represented in three states in the model, the reduced (red), semi reduced (semired) and oxidized (ox) form. The physiological concentrations are calculated for 1 mg chlorophyll (S3 Table). FDX was clamped to 50% reduced state. Estimated start values of FNR_{red} and $FNR_{semired}$ were each set to 40%. The oxidized form was initially set to 20%. Initial values of NTRC, FTR and TRX-f1 were 80% reduced and 20% oxidized. The initial 2CysPRX values were set to 35% reduced and 65% oxidized form [12]. The $NADPH/NADP^+$ couple started from a fully reduced state at t = 0. To mimic metabolic NADPH oxidation, the reaction constant v11 was added. (B-E) The redox states of the network components (B) FTR_{ox}, (C) TRX-f1, (D) FBPase, (E) 2CysPRX, (F,G) FNR, (H) NADPH, $NADP^+$ and (I) NTRC were simulated for 3h at constant H_2O_2 concentrations ranging from 0 µM to 100 µM.

https://doi.org/10.1371/journal.pcbi.1007102.g005

concentration dependencies of the redox states at first glance were rather similar between the individual and the combined models; however there were some striking differences with likely physiological significance. The TRX-f1 was still more reduced at 100 nM H_2O_2 in the combined than in the FTR model. Accordingly, the FBPase remained more reduced in the combined model still being 42% reduced at 100 nM H_2O_2 while it was close to 60% oxidized at 10 nM in the FTR model (cf. Figs 1 and 5).

The most striking difference was seen for 2CysPRX which was half oxidized at 3 nM H_2O_2 in the FTR model, but at slightly above 10 nM in the combined model. These important alterations in redox state after introducing the FNR branch witness the importance of the NTRC pathway in reducing 2CysPRX in line with published experimental results [9, 14]. The time-dependent changes in redox states of the network components (Fig 6) confirmed the critical range of the H_2O_2 concentration needed for stable redox states as also measurable *ex vivo*. Thus at 10 nM H_2O_2 in the combined model, there was a trend towards higher reduction, while clamping the H_2O_2 concentration to 100 nM reversed the trend toward higher oxidation of the network components.

The combined FTR/FNR-model allowed for estimating relative rates of electron drainage at competing branching points of the network and provided answers to the critical questions raised above. The first question addressed the estimation of the resting H_2O_2 concentration in the stroma *in vivo*. Several experimental studies have shown that the oxidized fraction of 2CysPRX exceeds that of the reduced fraction, e.g., [12] determined the ratio of oxidized to reduced forms to 65%:35%. Thus we asked our model at which clamped H_2O_2 concentration

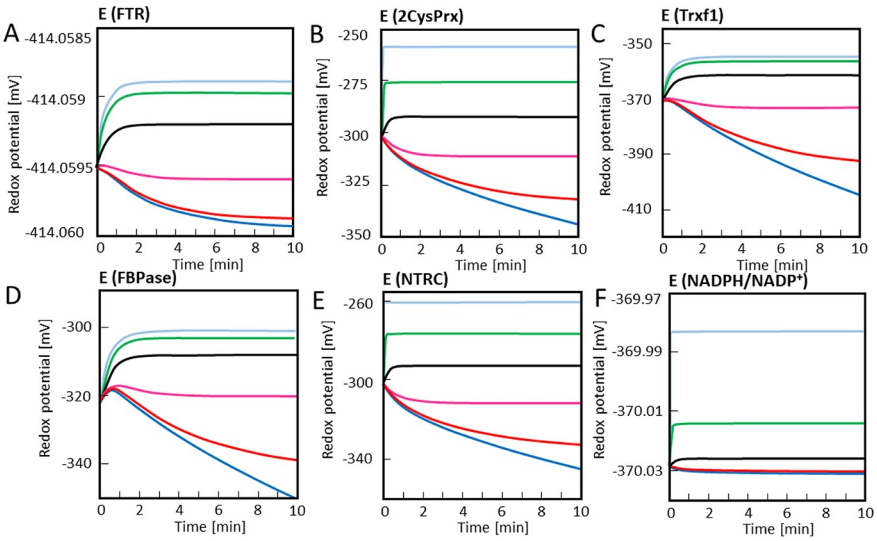

Fig 6. Time-dependent simulation of redox potentials of FTR/FNR-network components. The redox potentials of FTR/FNR-network components were simulated and included FDX, FNR, NADPH, NTRC, FTR, TRX-f1, FBPase and 2CysPRX. Redox potentials were calculated at each time step using the Nernst equation for (A) FTR, (B) 2CysPRX, (C) Trx-f, (D) FBPase, (E) NTRC and (F) NADPH/$NADP^+$ couple. The simulation was run for 10 min at constant H_2O_2 concentrations of 0 μM (blue), 1 nM (red), 10 nM (magenta), 100 nM (black), 1 μM (green) and 10 μM (cyan).

https://doi.org/10.1371/journal.pcbi.1007102.g006

this particular ratio is realized (S3 Table). The ratio of 65%:35% was established at 30 nM H_2O_2.

The second question concerned the ratio of electron flows from NADPH into metabolism (v11) and NTRC reduction (v9) assuming that only 2CysPRX acts as electron sink (Fig 7). For answering this question it was assumed that the H_2O_2 concentration in the resting state is close to 30 nM and then the simulated rate constants v9 and v11 and their ratios were computed (S4 Table). In this scenario, the electron flow into metabolism exceeded that into NTRC-dependent regeneration of 2CysPRX by a factor of 7410. The rate of regulatory electron flow reached only 0.14‰ of metabolic reduction. This value increased with increasing H_2O_2 in the simulation but did not exceed 5‰ even in the presence of 100 μM H_2O_2.

The third question dealt with the relative contribution of NTRC (v10) and TRX-f1 (v4) to reducing 2CysPRX (Fig 7). At low H_2O_2 concentrations v10 exceeded v4 by 2 to 3-fold; at 30 nM H_2O_2 the ratio of v10/v4 was 4.3. Apparently, the flux contribution of NTRC increased with increasing H_2O_2.

The final simulation explored the thermodynamic equilibrium between the NADPH system and the 2CysPRX mediated by NTRC. The ratio of NADPH/$NADP^+$ was varied between full reduction and full oxidation and the $2CysPRX_{red}/2CysPRX_{ox}$ computed assuming full equilibrium catalyzed by NTRC (Fig 8A). At a ratio of NADPH/$NADP^+$ = 1 only a small fraction of 2CysPRX was in the oxidized form (Fig 8A and 8B). Only at rather oxidized NADP system of 97.6% adjusted the 2CysPRX system at the ratio of 35% reduced and 65% oxidized as reported in photosynthesizing leaves [12]. The computing result was confirmed experimentally with recombinant proteins of NTRC and 2CysPRX equilibrated with varying NADPH/$NADP^+$-ratios, labeled with 5 mM N-ethylmaleimide polyethylene glycol ($mPEG_{mal}$) at pH 8 and separated on reducing sodium dodecylsulfate polyacrylamide gel electrophoresis (SDS-PAGE). The peroxidatic and resolving thiol of the reduced form bound two molecules of $mPEG_{mal}$ causing a shift of 10 kDa, while the disulfide bonded oxidized form could not be labeled and separated as a band at 20 kDa. In the presence of oxidized $NADP^+$, only the oxidized form of

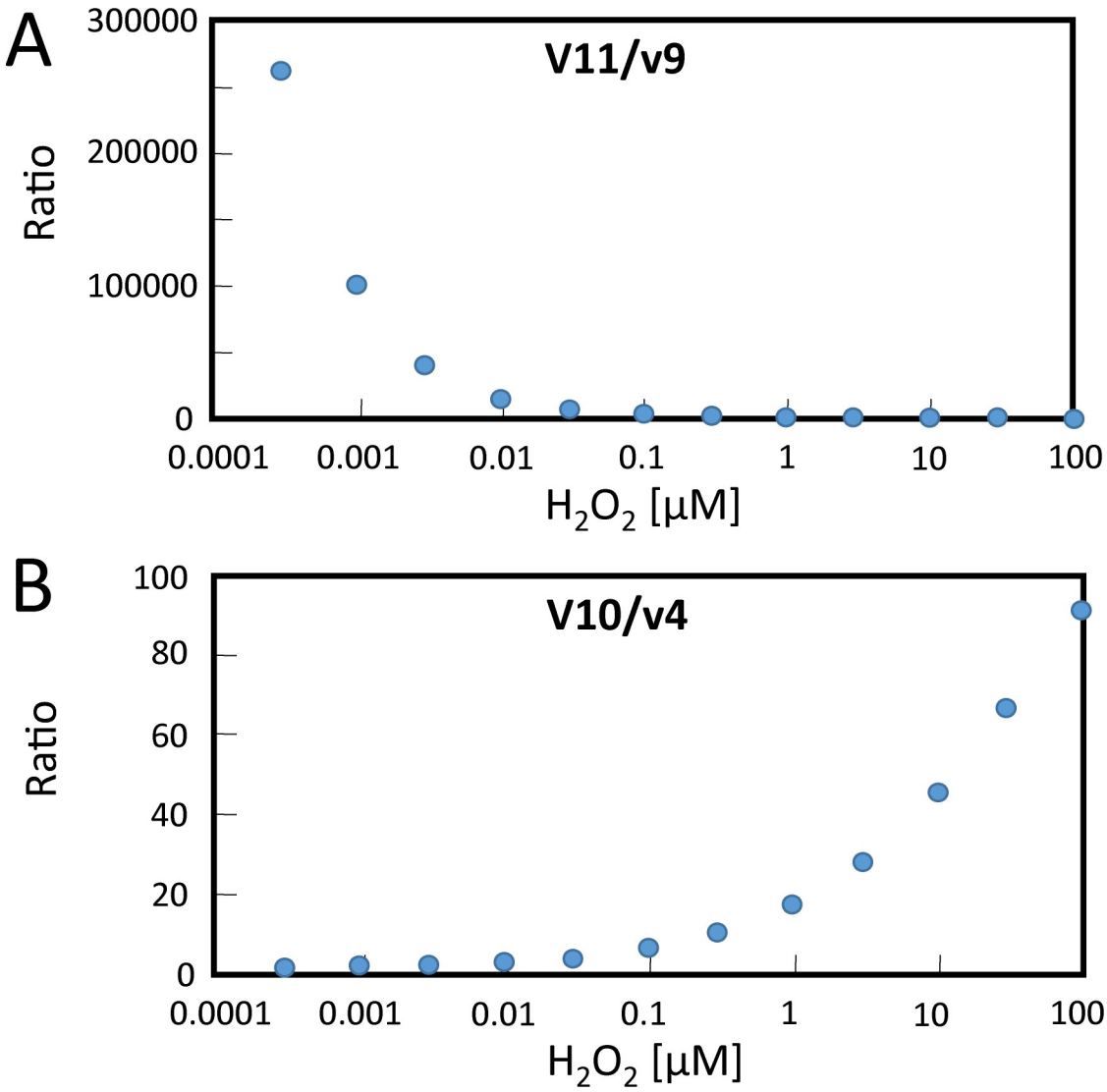

Fig 7. Steady state velocity ratios within the FTR/FNR network. Steady state velocities of the FTR/FNR-network (Fig 5A) were obtained after simulating the electron fluxes in the presence of various H_2O_2 concentrations. The physiological concentrations of network components were calculated for 1 mg chlorophyll. The H_2O_2 values were clamped in the simulation as given on the x-axis. (A) The ratio of the electron flux velocities from NADPH to metabolism (v11) relative to those from NADPH to thiol network (v9) were derived after 15 min. (B) Ratio of electron transfer rates from either TRX-f1 (v4) or NTRC (v10) to 2CysPRX as a function of clamped H_2O_2 concentrations.

https://doi.org/10.1371/journal.pcbi.1007102.g007

2CysPRX was observed. The oxidized form decreased with increasing NADPH/$NADP^+$-ratio. Importantly at a physiological NADPH/$NADP^+$-ratio of 1, a significant amount of $2CysPRX_{ox}$ was visible, albeit much less than 65% as reported [12].

Discussion

Redox and reactive oxygen species-dependent signaling is a general property of cells. For its understanding it is of fundamental importance to define the network connections, quantify electron fluxes and determine the driving forces [15]. Due to the network character, redox signaling can hardly be fully addressed experimentally. Thus work with mutants devoid of single and multiple network elements have provided important clues on their potential roles and

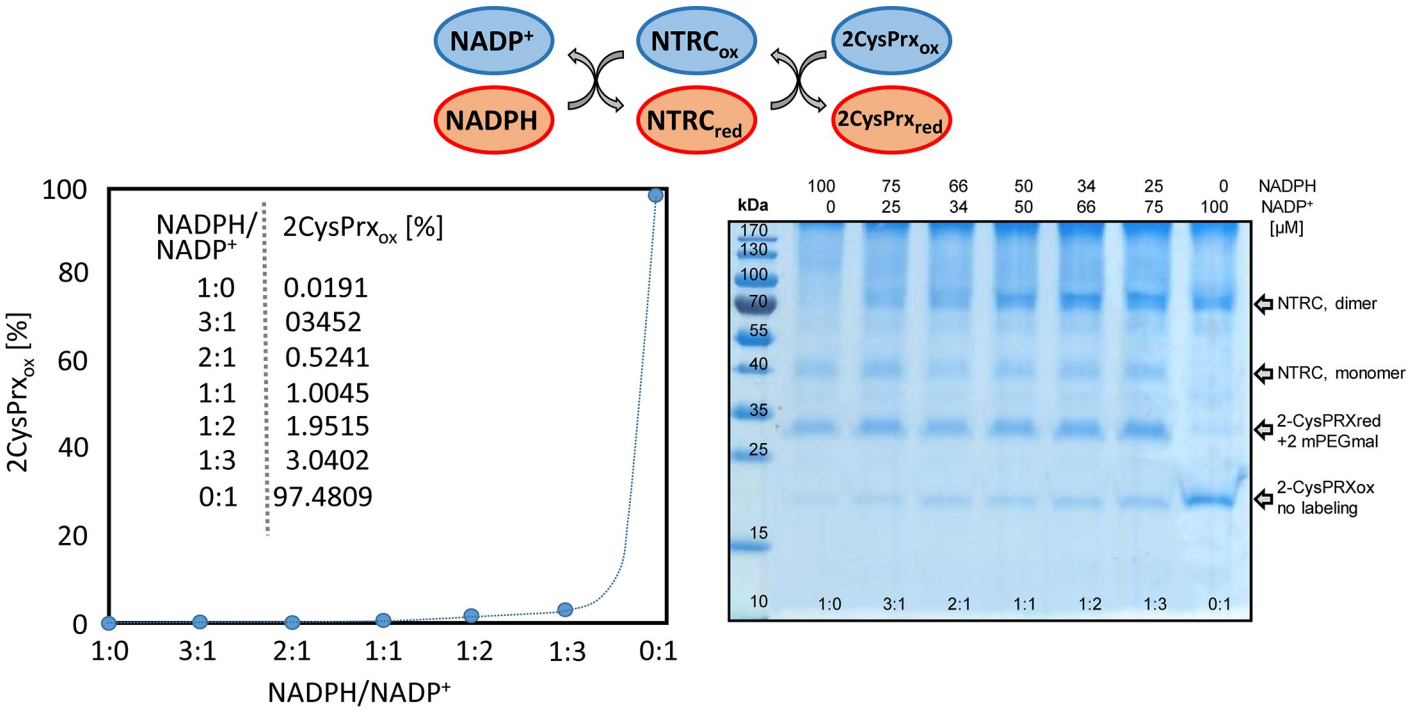

Fig 8. Redox equilibrium between NADPH and 2CysPRX catalyzed by NTRC as computed *in silico* and measured experimentally in the reconstituted system. (left figure) The equilibrium between varying NADPH/$NADP^+$-ratios and 2CysPRX was computed using a mathematical model consisting of differential equations (A.14, A.18, A.19). The concentration of components exhibits the values form the enzyme assay. (right figure) Enzymatic assays containing 10 μM NTRC, 5 μM 2CysPRX and 100 μM total (NADPH / $NADP^+$) in TRIS-buffer, pH 8, were incubated for 5 min. After labeling the free thiols with mPEG-maleimide which causes an increase in molecular mass by 5 kDa per introduced label, thus 10 kDa for two thiols, samples were separated by SDS-PAGE and visualized by Coomassie-silver staining. The positions in the gel of the oxidized (no label) and reduced forms (two labels) of 2CysPRX are indicated.

https://doi.org/10.1371/journal.pcbi.1007102.g008

functions, but also bear the problem of cumulating and equivocal effects [16,17]. For this reason, this study realized a computational approach for simulating two separate sub-networks and a combined network of the chloroplast as a meaningful approach complementary to the empiric avenue. In the following we will discuss the main conclusions drawn from our simulations and also address the potential shortcomings.

The contribution of NTRC to 2-CysPRX reduction exceeds that of the TRX-f-pathway

The FDX-FTR-branch was used to simulate the distribution of electrons between activation of an exemplary target protein, the chloroplast FBPase, and reduction of 2CysPRX. The FBPase is only one of several targets of TRX-f1 [16]. *Arabidopsis thaliana* lacking TRX-f1 lacks an obvious phenotype. However, the double mutant *ntrc*/*trx-f1* is compromised in multiple parameters such as growth, photosynthetic carbon assimilation and activation of FBPase. This is in line with our simulation results using the individual and combined models since either branch was able to reduce 2-CysPRX. The increased NADPH/NADP-ratio in the double mutant indicates an inhibition of CBB activity [16]. But even the double mutant *trx-f1*/*trx-f2* showed a significant reduction of the FBPase and RubisCO activase protein, indicating alternative pathways for the reduction of photosynthesis-related target enzymes. It is noteworthy that this simplified network allowed for simulating the data from the corresponding enzyme test surprisingly well [12]. The kinetic data of the network consisting of TRX-f1, FBPase and 2CysPRX either reconstituted from recombinant proteins in a test tube or computed in silico matched

with a regression coefficient of $R^2 = 0.998$. This 'perfect' match confirms the reliability of these particular reaction constants.

The model cannot reflect the complexity of the chloroplast TRX system which consists of 20 TRX and TRX-like proteins (Trx-m (4) +Trx-x (1) + Trx-y (2) +Trx-f (2) + Trx-z (1) + Trx-Like2 (2) + Trx-Lilium (5) + CDSP32 (1) + HCF164 (1) + NTRC (1)) and the NTRC [3,18]. The implementation of additional TRXs in the model would require quantitative data on their stromal concentration and affinity toward targets of interest. However this information is unavailable for most chloroplast TRXs. It is an interesting perspective that such interactions may be predicted based in electrostatic and geometric properties of the complementary interfaces of redox transmitter and redox target in the future [19].

The FNR branch provides electrons from PET to NADPH which is mainly consumed in the CBB. NADPH also reduces NTRC. The simulation gave a 5.46-fold higher contribution of the NTRC pathway to 2-CysPRX reduction than the TRX-f pathway. The reconstitution of NADPH/NTRC/2CysPRX system showed the reversibility and equilibrium in this pathway. A highly oxidized NADP system oxidizes 2CysPRX via NTRC. The data of Fig 8 show that even in the presence of 75% oxidized NADP-system, only a small fraction of 2-Cys PRX turns oxidized. This result was in line with the theoretical computation of the redox equilibrium. Reverse flow from 2CysPRX for $NADP^+$ reduction will only occur if the NADP-system is oxidized to an overwhelming fraction which rarely occurs. Such a far-going oxidation of the NADPH/$NADP^+$-ratio was reported for spinach leaves when lowering the steady state light intensity from 250 μmol photons$\cdot m^{-2}\cdot s^{-1}$ to 25 μmol photons$\cdot m^{-2}\cdot s^{-1}$ [20]. Thus the backflow may be a feedback mechanism upon sudden lowering or extinguishing the photosynthetic active radiation. After such a light step down, the CBB still consumes NADPH and strongly oxidizes the NADP-system, which oxidizes the 2CysPRX by backflow. This mechanism will accelerate the TRX oxidation by 2CysPRX acting as TRX oxidase [12] and thereby downregulates the CBB activity to readjust the NADPH/$NADP^+$-ratio to reach an energetic equilibrium.

The resting H_2O_2 concentration of the chloroplast is in the lower nanomolar range

Simulating the effect of H_2O_2 using the model combined from the FTR and FNR networks allowed for estimating velocities of empirically inaccessible reactions and amounts of resting H_2O_2 concentrations. Biochemical H_2O_2 determination in extracts or histochemical staining only provide rough estimates and possibly indications for alterations, but these quantifications give unrealistically high ROS amounts. Recent developments with H_2O_2-sensitive *in vivo* probes such as Hyper enable kinetic monitoring of H_2O_2 amounts in compartments of living cells. HyPer2 is a derivative of YFP fused to the H_2O_2 binding domain of the bacterial H_2O_2-sensitive transcription factor OxyR [21]. Using this sensor, Exposito-Rodriguez et al. [22] proved that chloroplast-sourced H_2O_2 likely are transported to the nucleus. The study exclusively was based on excitation ratios but H_2O_2 concentrations could not be estimated.

The steady state concentration of stromal H_2O_2 was approximated to about 30 nM in this study. The rational was to compare the electron distribution and computed redox states of network components in the presence of different H_2O_2 concentrations with reported data on the redox state of 2CysPRX *ex vivo* [9,12]. The high reaction rate of 2CysPRX with peroxide substrates [23] allows for rapid oxidation of the peroxidatic thiol and conversion to the disulfide form [24]. The limiting factor in the catalytic cycle is the regeneration [14,25]. The limited regeneration speed decreases the turnover number to values far below 1 s^{-1}. Consequently, any increase in H_2O_2 will shift the 2CysPRX redox state to more oxidation. The value of 30 nM could be an underestimation if other TRX isoforms or other electron donors significantly

contribute to the reduction of disulfide-bonded 2CysPRX. The most interesting candidate is TRX-x which proved to be the most efficient regenerator of 2CysPRX among the tested TRXs [7], but had little effect on the redox state of 2CysPRX measured *ex vivo* [9]. This may not be surprising since the fraction of TRX-x only amounts to 8% of that of TRX-f1 and 5% of that of NTRC in the stroma according to the AT_CHLORO mass-spectrometric protein database [26,27].

Electron flow for regulation amounts to a small fraction of metabolic reduction

Electrons from light-driven PET are distributed among different metabolic consumers such as carbon, nitrogen and sulfur assimilation which are serviced at a ratio of about 40:8:1. In addition part of the electrons are used for regulatory purposes, namely for producing both the reductants NADPH, glutathione and TRX as redox input elements into the thiol redox regulatory network [28] and the oxidant H_2O_2 [29]. The relative expenditure of reductive energy for redox regulation of the CBB cycle has been an open but unsolved issue for long, essentially since the discovery of TRXs. The mathematical simulation focusing on FBPase assumed that both the reductive and the oxidative driving forces are generated from PET. In this case and at a resting H_2O_2 concentration of 30 nM, metabolic electron drainage exceeds the NTRC-dependent regeneration of 2CysPRX by a factor of 7234-fold (S4 Table).

Considering the 5.46-fold lower electron flux from TRX-f1 to 2CysPRX than from NTRC at 30 nM H_2O_2 (S4 Table) the metabolic flux exceeds the reduction rate of 2CysPRX 6114-fold. An equivalent amount of electrons must be used to produce H_2O_2, increasing the reductive expenditure for FBPase redox regulation to $1/3057^{th}$ of metabolic flux. Considering the other redox regulated targets such as RubiCO activase, seduheptulose-1,7-bisphosphatase, glyceraldehyde-3-phosphate dehydrogenase, ribulo-5-phosphate kinase and malate dehydrogenase and assuming that regulation of these targets consumes, e.g., 30-fold more electrons than regulation of FBPase, then about 1% of the PET rate would be drained for redox regulation.

Another unknown parameter in the system is the nature of oxidation in addition to PET-derived H_2O_2. Two sources for oxidation should be taken into account. H_2O_2 is produced outside of the chloroplast, in the peroxisomes, in mitochondria and at the plasmamembrane by NADPH oxidases [30]. Antioxidant systems decompose these ROS and thus it is unlikely that external H_2O_2 penetrates the chloroplast and contributes to oxidation of redox target proteins. Another possible oxidant is elemental oxygen as suggested early after the discovery of thioredoxins. It would be important to obtain the kinetic data of O_2-mediated oxidation of TRX and other protein thiols in future work in order to incorporate such data in the mathematical model. Alternative oxidation reactions will increase the expenditure of electron for regulation.

The H_2O_2-dependency of the stromal redox state

The discussion up to this point concerned the steady redox state in the light. It is generally accepted that the rate of H_2O_2 generation increases in the chloroplast if exposed to excess excitation energy, in particular if coinciding with nutrient deficiency or low temperature. The combined model allows for analyzing the effect of changing H_2O_2 concentration. Increasing H_2O_2 will increase the oxidation state of the 2-CysPRX with immediate effects on the FTR/TRX system (Fig 5). It may be hypothesized that the concomitant downregulation of CBB and thus metabolic energy consumption frees energy for driving defense processes. In addition, the more oxidizing condition may activate the oxidative pentose phosphate cycle via glucose-6-phosphate dehydrogenase to provide additional reductive power for defense. Thus, the here presented model should be expanded to include both reductive activation and reductive

inhibition in order to understand the controlled readjustment of normal redox state. Naturally, one wishes to see experimental validations of the predictions: We are not aware of any experimental access to the three main estimates, the resting H_2O_2 concentration, the relative contribution of the TRX-f and NTRC pathway and the relative rates of electron fluxes into metabolism versus thiol regulation. The first two predictions appear highly reliable due to the immediate reaction of H_2O_2 with 2-CysPRX and the measured redox state of 2-CysPRX ex vivo on the one hand site, and the reported biochemical parameters on the other hand. The latter result is in good accordance with data from mutants and in vitro reconstitution experiments with recombinant proteins [9,14]. The third value concerning the electron flux into regulation gives a first estimate and will have to be substantiated by refinement of the mathematical model.

Materials and methods

Equilibrium between NADP-system and 2CysPRX catalyzed by NTRC

Hisx6-tagged recombinant NTRC and 2CysPRX were produced in *E. coli* and purified by Ni-nitrilotriacetic acid-based affinity chromatography as described [12]. 10 μM recombinant NTRC was incubated with 5 μM of 2CysPRXA and 100 μM NADPH/$NADP^+$ in 50 mM Tris-HCl pH 8 in a final volume of 50 μl for 5 min. Then 50 μl of TCA 20% (w/v) was added to the mixture and maintained on ice for 40 min. The assay mix was spun for 15 min at 13,000 rpm. The pellet was washed with TCA (2%, 100 μl). After 15 min centrifugation at 13 000 rpm, the pellet was resuspended with 15 μl of 50 mM Tris-HCl pH 7.9 containing mPEGmal with 1% SDS. After 90 min at room temperature, SDS-PAGE loading buffer with ß-mercaptoethanol was added. 20 μl of the mixture were separated by SDS-PAGE (12% w/v) and protein bands visualized with Coomassie-silver staining.

Concentrations of network components

Concentrations of chloroplast proteins were taken from literature and calculated for 1 mg Chl referred to 66 μl stroma [31] and 10 mg stromal protein. The calculated concentration values were summed for isoforms. In all models each H_2O_2 and FDX concentration were set constant. The start values of variables were partitioned into 80% of reduced and 20% of oxidized form except for FNR, 2CysPRX and NADPH/$NADP^+$ couple (S5 Table).

Model formulation

Three chloroplast network models were developed to analyze electron transfer rates as well as oxidized and reduced states of network components with various H_2O_2 concentrations. The first model describes the FTR-based electron transfer to 2CysPRX (Fig 1A). It is built on the previously published model of Vaseghi *et al.* [12] and describes the electron drainage in the presence of different H_2O_2 concentrations. The second model reveals the FNR-based electron transfer (Fig 3A) and the third model combines both models (Fig 5A).

A) FTR network model. In order to analyse the electron distribution from TRX-f1 to FBPase or 2CysPRX in dependence on H_2O_2 concentration, the first simplified model of the FTR network consisted of FDX, FTR, TRX-f1, FBPase, 2CysPRX and H_2O_2 (Fig 1A). FDX and H_2O_2 were constant parameters. FDX was fixed to 50% reduction and the H_2O_2 concentration varied from 0.3 nM to 10 μM. The four variables were FTR, TRX-f1, FBPase and 2CysPRX. Each variable could adopt the oxidized and reduced state. Electrons were transferred from FDX (v1) via FTR to TRX-f1 (v2). TRX-f1 distributed the electrons to FBPase (v3) and 2CysPRX (v4). H_2O_2 oxidized 2CysPRX (v5). The rate equations were implemented using mass action

law (S1A1 Text). The reactions were formulated as reversible second order rates (except v5).

$$v_4 = k_4 * ([Trxf1_{red}] * [2CysPrx_{ox}] - \frac{[Trxf1_{ox}] * [2CysPrx_{red}]}{K_{eq_T rxf12CP}}) \quad (1)$$

The transition from one electron transfer to two electron transfer takes place at FTR. Therefore, two FDX are required to reduce FTR.

$$v_1 = k_1 * ([FDX_{red}] * [FDX_{red}] * [FTR_{ox}] - \frac{[FDX_{ox}] * [FDX_{ox}] * [FTR_{red}]}{K_{eq_F dFTR}}) \quad (2)$$

B) FNR network model. The second model aimed to describe the reduction power in the FNR branch toward 2CysPRX and represents the electron transfer via FNR and NTRC (Fig 3A). This FNR network model consisted of FDX, FNR, NADPH, NTRC, 2CysPRX and H_2O_2. Each component exhibited two states in the model; oxidized and reduced form. Only FNR (the transition molecule from one to two electron transport) was represented in three forms; reduced, half reduced and oxidized. Electrons were transferred from FDX (constant reduced 50%) to FNRox (v6) that results in half reduced FNR form.

$$v_6 = k_{+6} * [FDX_{red}] * [FNR_{ox}] - k_{-6} * [FDX_{ox}] * [FNR_{semired}] \quad (3)$$

A further reduction by FDX of FNRsemired (v7) resulted in the fully reduced form of FNR (FNRred).

$$v_7 = k_{+7} * [FDX_{red}] * [FNR_{semired}] - k_{-7} * [FDX_{ox}] * [FNR_{red}] \quad (4)$$

FNRred transferred electrons to $NADP^+$ (v8) to produce NADPH. In order to mimic metabolic NADPH consumption an estimated rate of NADPH decrease was included (v11). In this network NADPH transferred electrons to NTRCox (v9) that led to reduced NTRC (NTRCred). The reduction of 2CysPRXox took place by NTRCred (v10). Reduced 2CysPRX reduced H_2O_2 to 2 H_2O (v5). H_2O_2 was included as a constant and varied from 0 nM to 100 μM. (S1B Text)

C) The combined FTR-FNR network model. To analyse the interaction between the FTR and FNR branch in adjusting the 2CysPRX and FBPase redox states in dependence on different H_2O_2 concentrations a third model was constructed consisting of the FTR and FNR networks (Fig 5A). All components except FDX and H_2O_2 were variables and represented in reduced and oxidized form. Only FNR adopted three different redox states; reduced, oxidized and half reduced.

The equilibrium constants K_{eq} in all reactions were calculated using the standard cell potentials E^o of each cell reaction at pH 7 linked to the standard reaction Gibbs energy $\Delta_R G^o$ [32]:

$$K_{eq} = exp(-\Delta_R G^o / RT) \text{ with } \Delta_R G^o = -nF \cdot E^o \quad (5)$$

where R is the gas constant, T the thermodynamic temperature, F the Faraday constant and n the stoichiometric coefficient of the electrons in the half-reactions in which the cell reaction can be divided. The models were formalized as systems of differential equations (S1C Text). Steady-state solutions were computed numerically in MATLAB.

Calculation of redox potentials

Redox potentials were calculated at each time step using the Nernst equation at room temperature

$$E = E^0 + \frac{0.059V}{z} log_{10} \frac{[ox]}{[red]} \quad (6)$$

where E is the redox potential, E^0 the standard cell potential at pH = 7 (S1D Text), z the stoichiometric coefficient of the electrons in the half-reactions and [ox] and [red] the concentration of the oxidized and reduced form of the component, respectively.

Fitting of unknown parameter

Three unknown parameters were fitted to data [33]. A fourth model was developed containing all components of the measurements. The network consisted of NADPH (0.5 mM), FNR (0.2 μM), FDX (1 μM), FTR (1μM), TRX-f1 (2μM) (S4 Fig).

Because the initial values of the parameters were not available, we have decided for global optimization algorithm (MATLAB Genetic Algorithm Tool, GA). Since GA requires a lot of computing capacity, the output parameters were not always accurate. Here we used the output parameters of the GA-optimization at different local minima as the initial guess. Local algorithms could calculate the parameters more correctly (S1C Text, S5 Fig). For a comparison, we applied the two MATLAB local algorithms: "fminunc" and "lsqnonlin". All the final parameters of the paper are results of the global and local optimization. As a measure of the sensitivity values of the fval function to the each fitted parameter, k+1, k+2 and k-8, we used the rates of convergence of the fval-value to minima in respect of variations of each of the parameters. See S1 Text, table C1 and S6 Fig for the minima.

In order to mimic the physiological behavior of the chloroplast an overall rate constant was estimated and included the rate of metabolic electron drainage from NADPH (v11). Studies of NADPH/$NADP^+$ concentrations in the light reports a ratio of 50% [34]. The network without the constant leads to 90% of NADPH and 10% $NADP_+$(S1 Fig). The constant v11 was manual fitted. The NADPH concentration after inclusion of v11 stays at approximately 50% ±0.2 at all H_2O_2 concentrations (Fig 3A).

Supporting information

S1 Text. Compilation of all equations used in the redox network models and description and fitting of the biochemical parameters.
(PDF)

S1 Fig. Simulated steady state of FNR-network components in dependence on H_2O_2 concentrations in the absence of electron drainage by metabolism.
(TIFF)

S2 Fig. Simulation of time-dependent redox potential changes of FNR-network components in the absence of metabolic electron drainage.
(TIFF)

S3 Fig. Model comparison by simulation of model components over time.
(TIFF)

S4 Fig. Fitting of unknown parameter.
(TIFF)

S5 Fig. Fitting of unknown parameter—Results.
(TIFF)

S6 Fig. Fitting of unknown parameters–sensitivity of fval function.
(TIFF)

S1 Table. Simulated steady state concentrations of FTR-network components.
(TIFF)

S2 Table. Simulated steady redox state of the FNR-network components.
(TIFF)

S3 Table. Simulated steady state concentrations of the FTR/FNR-network components.
(TIFF)

S4 Table. Calculated ratios of steady state velocities observed in the combined FTR/FNR-network.
(TIFF)

S5 Table. Distribution of network components in reduced and oxidized form at t = 0 in FTR-FNR model.
(TIFF)

S6 Table. Reaction equations describing the model of FTR network model.
(TIFF)

S7 Table. Reaction equations describing the model of FNR network model.
(TIFF)

S8 Table. Reaction equations describing the model of the combined FTR-FNR network model.
(TIFF)

S1 MATLAB Files. Files for modelling the FTR, FNR and FTR/FNR models in MATLAB, including the information on parameters and fitting procedures.
(RAR)

Author Contributions

Conceptualization: Melanie Gerken, Karl-Josef Dietz.

Data curation: Melanie Gerken, Sergej Kakorin.

Formal analysis: Melanie Gerken, Sergej Kakorin.

Funding acquisition: Karl-Josef Dietz.

Investigation: Melanie Gerken.

Project administration: Karl-Josef Dietz.

Resources: Karl-Josef Dietz.

Supervision: Karl-Josef Dietz.

Validation: Kamel Chibani.

Visualization: Melanie Gerken.

Writing – original draft: Melanie Gerken, Karl-Josef Dietz.

Writing – review & editing: Melanie Gerken, Sergej Kakorin, Kamel Chibani, Karl-Josef Dietz.

References

1. Hanke G, Mulo P. Plant type ferredoxins and ferredoxin-dependent metabolism. Plant Cell Environ. 2013; 36: 1071–1084. https://doi.org/10.1111/pce.12046 PMID: 23190083
2. Serrato AJ, Pérez-Ruiz JM, Spínola MC, Cejudo FJ. A novel NADPH thioredoxin reductase, localized in the chloroplast, which deficiency causes hypersensitivity to abiotic stress in *Arabidopsis thaliana*. J. Biol. Chem. 2004; 279: 43821–43827. https://doi.org/10.1074/jbc.M404696200 PMID: 15292215
3. Meyer Y, Reichheld JP, Vignols F. Thioredoxins in Arabidopsis and other plants. Photosynth. Res. 2005; 86: 419–433. https://doi.org/10.1007/s11120-005-5220-y PMID: 16307307
4. Gütle DD, Roret T, Müller SJ, Couturier J, Lemaire SD, Hecker A, Dhalleine T, Buchanan BB, Reski R, Einsle O, Jacquot JP. Chloroplast FBPase and SBPase are thioredoxin-linked enzymes with similar architecture but different evolutionary histories. Proc. Natl. Acad. Sci. USA. 2016; 113: 6779–6784. https://doi.org/10.1073/pnas.1606241113 PMID: 27226308
5. Hashida SN, Miyagi A, Nishiyama M, Yoshida K, Hisabor T., Kawai-Yamada M. Ferredoxin/thioredoxin system plays an important role in the chloroplastic NADP status of Arabidopsis. Plant J. 2018; 95: 947–960. https://doi.org/10.1111/tpj.14000 PMID: 29920827
6. Scheibe R. $NADP^+$-malate dehydrogenase in C-3-plants–Regulation and role of a light-activated enzyme. Physiol. Plant. 1987; 71: 393–400.
7. Collin V, Issakidis-Bourguet E, Marchand C, Hirasawa M, Lancelin JM, Knaff DB, Miginiac-Maslow M. The Arabidopsis plastidial thioredoxins: new functions and new insights into specificity. Journal of Biological Chemistry. 2003; 278: 23747–23752. https://doi.org/10.1074/jbc.M302077200 PMID: 12707279
8. Dangoor I, Peled-Zehavi H, Levitan A, Pasand O, Danon A. A small family of chloroplast atypical thioredoxins. Plant Physiol. 2009; 149: 1240–1250. https://doi.org/10.1104/pp.108.128314 PMID: 19109414
9. Pulido P, Spínola MC, Kirchsteiger K, Guinea M, Pascual MB, Sahrawy M, Sandalio LM, Dietz KJ, González M, Cejudo FJ. Functional analysis of the pathways for 2-Cys peroxiredoxin reduction in *Arabidopsis thaliana* chloroplasts. Journal of Experimental Botany. 2010; 61: 4043–4054. https://doi.org/10.1093/jxb/erq218 PMID: 20616155
10. Collin V, Lamkemeyer P, Miginiac-Maslow M, Hirasawa M, Knaff DB, Dietz KJ, Issakidis-Bourguet E. Characterization of plastidial thioredoxins from Arabidopsis belonging to the new y-type. Plant Physiology. 2004; 136: 4088–4095. https://doi.org/10.1104/pp.104.052233 PMID: 15531707
11. Dietz KJ. Thiol-Based Peroxidases and Ascorbate Peroxidases: Why Plants Rely on Multiple Peroxidase Systems in the Photosynthesizing Chloroplast? Mol Cells. 2016; 39: 20–25. https://doi.org/10.14348/molcells.2016.2324 PMID: 26810073
12. Vaseghi MJ, Chibani K, Telman W, Liebthal MF, Gerken M, Schnitzer H, Mueller SM, Dietz KJ. The chloroplast 2-cysteine peroxiredoxin functions as thioredoxin oxidase in redox regulation of chloroplast metabolism. Elife. 2018; 7: e38194. https://doi.org/10.7554/eLife.38194 PMID: 30311601
13. Wenderoth I, Scheibe R, von Schaewen A. Identification of the cysteine residues involved in redox modification of plant plastidic glucose-6-phosphate dehydrogenase. Journal of Biological Chemistry. 1997; 272: 26985–26990. https://doi.org/10.1074/jbc.272.43.26985 PMID: 9341136
14. Muthuramalingam M, Seidel T, Laxa M, Nunes de Miranda SM, Gärtner F, Ströher E, Kandlbinder A, Dietz KJ. Multiple redox and non-redox interactions define 2-Cys peroxiredoxin as a regulatory hub in the chloroplast. Molecular Plant. 2009; 2: 1273–1288. https://doi.org/10.1093/mp/ssp089 PMID: 19995730
15. Jacquot JP, Dietz KJ, Rouhier N, Meux E, Lallement PA, Selles B, Hecker A. Redox regulation in plants: glutathione and "redoxin" related families. In: Oxidative Stress and Redox Regulation, Jakob U, Reichmann D. eds. Springer, Dordrecht. 2013; 213–231.
16. Thormählen I, Meitzel T, Groysman J, Öchsner AB, von Roepenack-Lahaye E, Naranjo B, Cejudo FJ, Geigenberger P. Thioredoxin f1 and NADPH-Dependent Thioredoxin Reductase C Have Overlapping Functions in Regulating Photosynthetic Metabolism and Plant Growth in Response to Varying Light Conditions. Plant Physiology. 2015; 169; 1766–1786. https://doi.org/10.1104/pp.15.01122 PMID: 26338951
17. Naranjo B, Diaz-Espejo A, Lindahl M, Cejudo FJ. Type-f thioredoxins have a role in the short-term activation of carbon metabolism and their loss affects growth under short-day conditions in Arabidopsis thaliana. Journal of Experimental Botany. 2016; 67: 1951–1964. https://doi.org/10.1093/jxb/erw017 PMID: 26842981

18. Chibani K, Wingsle G, Jacquot JP, Gelhaye E, Rouhier N. Comparative genomic study of the thioredoxin family in photosynthetic organisms with emphasis on *Populus trichocarpa*. Molecular Plant. 2009; 2 (2): 308–322. https://doi.org/10.1093/mp/ssn076 PMID: 19825616

19. Berndt C, Schwenn JD, Lillig CH. The specificity of thioredoxins and glutaredoxins is determined by electrostatic and geometric complementarity. Chemical Science. 2015; 6: 7049–7058. https://doi.org/10.1039/c5sc01501d PMID: 29861944

20. Prinsley RT, Dietz KJ, Leegood R. Regulation of photosynthetic carbon assimilation in spinach leaves after a decrease in irradiance. Biochimica et Biophysica Acta. 1986; 849: 254–263.

21. Belousov VV, Fradkov AF, Lukyanov KA, Staroverov DB, Shakhbazov KS, Terskikh AV, Lukyanov S. Genetically encoded fluorescent indicator for intracellular hydrogen peroxide. Nature Methods. 2006; 3: 281–286. https://doi.org/10.1038/nmeth866 PMID: 16554833

22. Exposito-Rodriguez M, Laissue PP, Yvon-Durocher G, Smirnoff N, Mullineaux PM. Photosynthesis-dependent H_2O_2 transfer from chloroplasts to nuclei provides a high-light signalling mechanism. Nature Communication. 2017; 8(1): 49.

23. Brigelius-Flohé R, Flohé L. Basic principles and emerging concepts in the redox control of transcription factors. Antioxidants and Redox Signaling. 2011; 15: 2335–2381. https://doi.org/10.1089/ars.2010.3534 PMID: 21194351

24. König J, Baier M, Horling F, Kahmann U, Harris G, Schürmann P, Dietz KJ. The plant-specific function of 2-Cys peroxiredoxin-mediated detoxification of peroxides in the redox-hierarchy of photosynthetic electron flux. Proceedings of the National Academy of Science USA. 2002; 99: 5738–5743.

25. König J, Lotte K, Plessow R, Brockhinke A, Baier M, Dietz KJ. Reaction mechanism of the 2-Cys peroxiredoxin: Role of the C-terminus and the quarternary structure. Journal Biological Chemistry. 2003; 278: 24409–24420.

26. Ferro M, Brugière S, Salvi D, Seigneurin-Berny D, Court M, Moyet L, Ramus C, Miras S, Mellal M, Le Gall S, Kieffer-Jaquinod S, Bruley C, Garin J, Joyard J, Masselon C, Rolland N. AT_CHLORO, a comprehensive chloroplast proteome database with subplastidial localization and curated information on envelope proteins. Molecular & Cellular Proteomics. 2010; 9: 1063–1084.

27. König J, Muthuramalingam M, Dietz KJ. Mechanisms and dynamics in the thiol/disulfide redox regulatory network: transmitters, sensors and targets. Current Opinion in Plant Biology. 2012; 15: 261–268. https://doi.org/10.1016/j.pbi.2011.12.002 PMID: 22226570

28. Dietz KJ. Redox signal integration: From stimulus to networks and genes. Physiol Plantarum. 2008; 133: 459–468.

29. Driever SM, Baker NR. The water-water cycle in leaves is not a major alternative electron sink for dissipation of excess excitation energy when CO2 assimilation is restricted. Plant, Cell and Environment. 2011; 34: 837–846. https://doi.org/10.1111/j.1365-3040.2011.02288.x PMID: 21332508

30. Foyer CH, Noctor G. Redox signaling in plants. Antioxidants & Redox Signalling. 2013; 18: 2087–2090.

31. Winter H, Robinson DG, Heldt HW. Subcellular volumes and metabolite concentrations in spinach leaves. Planta. 1994; 193: 530–535.

32. Poughon L, Dussap CD, Gros JB. Energy Model and Metabolic Flux—Analysis for Autotrophic Nitrifiers. Biotechnology and Bioengineering. 2001; 72: 416–433. PMID: 11180062

33. Yoshida K, Hisabori T. Distinct electron transfer from ferredoxin-thioredoxin reductase to multiple thioredoxin isoforms in chloroplast. Biochemical Journal. 2017; 474: 1347–1360. https://doi.org/10.1042/BCJ20161089 PMID: 28246333

34. Heber U, Santarius KA. Compartmentation and reduction of pyridine nucleotides in relation to photosynthesis. Biochim Biophys Acta. 1965; 109: 390–408. https://doi.org/10.1016/0926-6585(65)90166-4 PMID: 4379647